UV laser pulse temporal profile requirements for the LCLS injector - Part I - Fourier Transform limit for a temporal zero slope flattop

C. Limborg-Deprey and P.R. Bolton,
Stanford Linear Accelerator Center,
MS 18, 2575 Sand Hill Road
Menlo Park, California 94025.

Abstract:
The temporal profile of the uv drive laser pulse for the LCLS injector is specified by the duration, the rise/fall time, and the maximum rms amplitude (for all frequencies) of residual modulation in the plateau region. The bandwidth of the uv laser system should accommodate pulses with a rise/fall time as low as 0.7 ps and an rms residual amplitude modulation (on the plateau) below 0.5% in the absence of a laser heater. Computations including the laser heater [3] relax this requirement to the 5% level. Numerical analyses of Fourier transform limited uv pulses show that the extent of frequency sidebands should extend to at least 1.5 THz on either side of the central uv frequency. For simplicity, we assume that the emitted electron beam profile matches the laser profile. The evolution of those electron beam distributions in the longitudinal phase space along the beamline as calculated with PARMELA/ASTRA are shown.
Related spectral and shaping requirements on the fundamental ir pulses are briefly addressed.

I - Introduction:

For reaching gain saturation at 1.5-A in the LCLS FEL, the slice emittance of the electron beam needs to be less 1.2 μm, the peak current more than 3.4 kA, and the slice energy spread smaller than 2.10^{-4} at the entrance of the undulator. To reach those goal parameters, the injector has to provide a beam with slice emittance smaller than 1 μm and a projected emittance of less than 1.2 μm for a 1nC, 10ps long electron bunch. A slice emittance corresponds to the emittance of particles contained in a longitudinal slice whose length is 1% of the total bunch length. The choice of 1% slices along the bunch has been chosen because it is the cooperation length in the undulator during the Self_Amplification of SpontaneousEmission (SASE)..
In order to accommodate emittance growth in the linac and bunch compressors, emittance values targeted for the injector are obviously more restrictive than those required at the entrance of the undulator. Accordingly, the emittance values targeted at the end of the injector, with computations performed for an idealized machine, are in fact less than 1.0μm for the projected emittance and less than 0.9μm for the 80%-emittance, leaving some room for the emittance growth due to field errors[1].

The next paragraph defines the various emittance quantities. It can be skipped by the person familiar with them.
The total projected emittance is given by

$\varepsilon_{proj.} = \sqrt{\langle x_i^2 \rangle \langle p_{xi}^2 \rangle - \langle x_i p_{xi} \rangle^2}$ in which the quantities <> are averaged over all particles i in the bunch. The 80%-emittance is computed using averaging over the particles contained in the 80 core slices out of 100 longitudinal slices along the bunch. It can be expressed similarly as

$\varepsilon_{80} = \sqrt{\langle x_i^2 \rangle \langle p_{xi}^2 \rangle - \langle x_i p_{xi} \rangle^2}$ where the i particles are contained in slices numbered 10 to 90.

The slice emittance, $\varepsilon_{slice,j}$ is computed for the quantities averaged over a single longitudinal slice. We then have $\varepsilon_{slice,j} \sqrt{\langle x_i^2 \rangle \langle p_{xi}^2 \rangle - \langle x_i p_{xi} \rangle^2}$ where the i particles are contained in a single slice j. In table 1, we computed the average of the slice emittance $<\varepsilon_{slice,j}>$, first for the slice number j from 10 to 90, and second for the slice number 1 to 100. The average of the slice emittances is smaller than the projected emittance because the slices are mismatched in the(x, p_x) phase space.

The LCLS accelerator systems have been optimized for minimizing both the total projected emittance and the slice emittance with the understanding that the slice emittance value is the critical one in the SASE process. Indeed, a good matching of the beam along this accelerator is only possible if the total projected emittance is relatively small. The projected emittance is also the quantity most easily measured. The difference between the slice emittance and the projected emittance comes principally from the particles contained in the head and tail of the bunch. Those particles do not meet the current and emittance conditions to drive SASE. To summarize the emittance quality of the beam in a single number, we therefore prefer to quote the 80%-emittance which gives slice emittance information on the useful part of the beam.

The 80%-emittance is limited in part by imposing longitudinal specifications on the temporal or power profile of the uv pulse that irradiates the RF gun's photocathode; specifically, the rise and fall time as well as the amplitude noise in the plateau region. The nominal uv pulse is longitudinally flattopped with a duration (FWHM) of 10 psec and a rise / fall time interval (10% to 90% levels) of 0.7 psec. As shown in table1, only a rise/fall time of less than 0.7 ps gives an 80% emittance of less than 0.9μm. However, simulations show that a 0.9 μm slice emittance (10% to 90% averaged case) can be obtained for rise/fall times in the range of 0.5 to 1.5 psec.

Rise/fall	0.7 ps	1.0ps	1.5 ps
$\varepsilon_{projected}$ [mm.mrad]	0.954	1.028	1.141
$\varepsilon_{80\%}$ [mm.mrad]	0.894	0.935	0.986
$<\varepsilon_{slice}>_{10..90}$[mm.mrad]	0.849	0.877	0.901
$<\varepsilon_{slice}>_{1..100}$[mm.mrad]	0.906	0.953	1.004

Table 1- Emittance values for three rise/fall times. We list the projected emittance the 80%-emittance, the average of the slice emittances for slice number10 to 90, and the average of the slice emittances for slice number 1 to 100

. The maximum allowed modulation amplitude on the longitudinal plateau of the uv pulse is limited by: (i) the maximum slice emittance value and (ii) detrimental effects of the longitudinal space charge (LSC) instability which are sensitive to the modulation periodicity.

The LSC instability has been thoroughly studied (see references [1,2,3,4]). It was shown that the rms amplitude of modulation should not exceed 0.5% for modulation periodicities longer than 50μm when no laser heater is considered. With the laser heater, the modulation amplitude should not exceed 5%. These two values, 0.5% and 5%, are reference levels for this report.

We consider the transform limited amplitude and periodicity of superimposed sinusoidal modulations on the flat plateau that are determined uniquely by the single pulse frequency spectrum for a given rise/fall time. Although the detailed uv pulse specifications allow for a plateau of nonzero slope, we address a zero slope case for this Part 1 report (the non-zero slope case is addressed in a Part II). The periodicities and amplitudes of sinusoidal modulations are established by the frequency limits or spectral cutoffs imposed on the sideband envelope spectrum (about some nominal central value). The periodicity of the amplitude ripple is to be distinguished from the wavelength bandwidth that is determined from the frequency bandwidth and whose magnitude is given by:

$$\Delta\lambda = \lambda^2 \frac{\Delta\nu}{c} \qquad (1)$$

II – Methodology and Pulse Shape Model :

The temporal profile of the uv pulse has been modeled using a Fermi-Dirac type distribution, $g(t)$ given by [5]:

$$g(t) = g_o \frac{1}{1+e^{\frac{|t|-to}{W}}} = g_o \frac{1}{1+e^{\beta\left(\frac{|t|}{t_o}-1\right)}}$$

$$\text{with } g_o^{-1} \approx \pi t_o^2 \left\{\left[\frac{1}{1+e^{-\beta}}+\frac{\pi^2}{3\beta^2}\right]+O\left(\frac{1}{\beta^4}\right)\right\} \quad (2)$$

where the profile is symmetric about t=0 and:

$\beta = t_o/W$	31.5	21.9	14.6
Rise/Fall (10-90%)	0.7 ps	1 ps	1.5 ps
t_o (HWHM)	5.0 ps	5.0 ps	5.0 ps

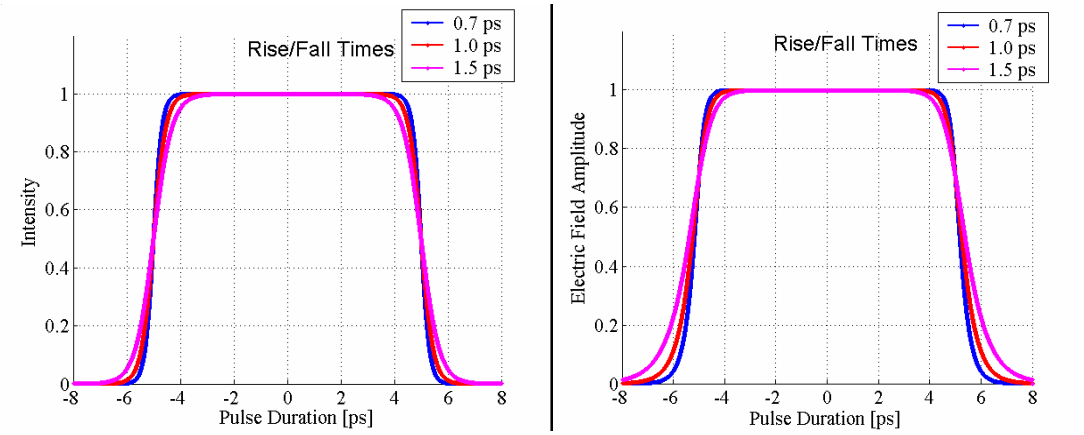

Figure 1a- Intensity and Electric Field profiles based on Fermi-Dirac function with different rise/fall times

Maintaining the FWHM at 10 psec, we generated three pulse profiles representing rise/fall times of 0.7, 1.0, and 1.5 psec. These are illustrated in figure 1a. The rise/fall time (10% to90% level) is approximately equal to 23% of W in the above table.

The power spectra have a sinc^2 functional form as shown in the corresponding positive sidebands plotted in figure 1b (using both linear and logarithmic scales). The nominal central frequency (near 1,175 THz for the central uv wavelength of 255nm and 392 THz for the central ir wavelength of 765 nm) has been subtracted to facilitate display of the sidebands). These are envelope spectra and the frequency scale is therefore a frequency difference scale. The spacing between sideband peaks and also between consecutive minima is equal to the inverse FWHM which is 0.1 THz. The central peak value (at the origin) has been normalized to one to illustrate the relative significance of sideband amplitudes.

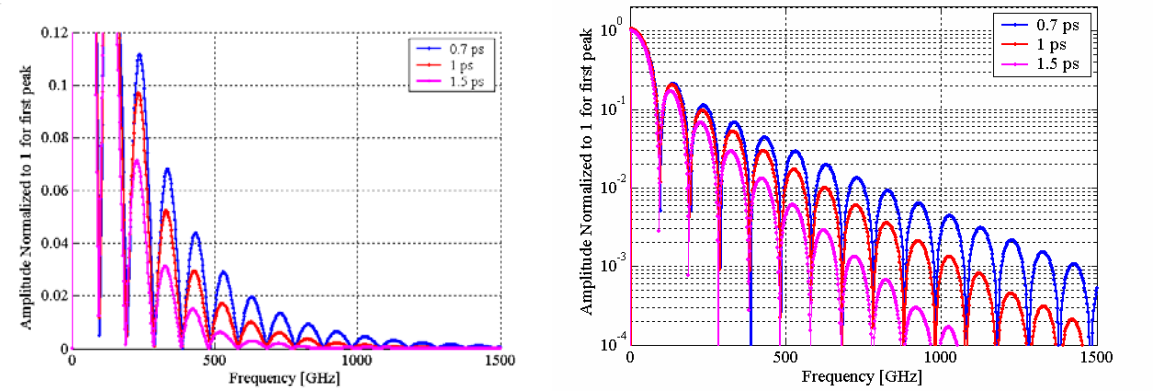

Figure1b-
Left plot - Fourier transform of the single pulse envelope with the central lobe amplitude normalized to 1
Right plot - same as the left plot except with a logarithmic ordinate.

The sideband amplitude diminishes with increased frequency. Furthermore, the relative amplitude of a given sideband at some fixed frequency diminishes with increasing rise/fall time. For example, for a 0.7 psec rise/fall time and a positive sideband frequency that is about 1.1 THz above the central value, the relative peak amplitude is $5x10^{-3}$ which is about twenty –five times greater than the corresponding value for a 1.5 ps rise/fall time.

Consequently the extent to which the ideal Fermi-Dirac temporal profile with a true 'flattop' plateau can be frequency 'synthesized' depends on the finite extent of the spectral bandwidth and therefore the number of sidebands that it contains. We specify this extent by imposing an abrupt cutoff value for the positive sidebands. In this report, the frequency cutoff value is the half bandwidth value. In all cases the negative sidelobes are cut symmetrically such that the full bandwidth is then twice this cutoff value. We computed the temporal characteristics of frequency synthesized uv pulses by inverse Fourier transforming spectra that have been cropped this way. The 5 steps of the computation are therefore:

1- Computed the electrical field amplitude temporal profile (square root of intensity temporal profile)
2- Perform Fourier transform
3- Truncate the Bandwidth
4- Perform the inverse Fourier transform to recover an electrical field amplitude temporal profile
5- Convert the electrical field amplitude temporal profile back to an intensity temporal profile (square the field profile)

III Results of Frequency Syntheses :

(a) Amplitude Modulation on the Plateau

Figures 2a and 2b show typical results of cropping sideband spectra for the 1.0 psec rise/fall time case. Results from cutoff values from 0.29 THz to 0.68 THz are displayed. These values correspond to sideband nodes. As anticipated, higher cutoff values transform to temporal profiles with lower longitudinal periodicity (higher frequency) and lower modulation amplitude on the plateau. For a 1 THz cutoff the amplitude ripple on the plateau has a longitudinal periodicity near 300 microns as expected.

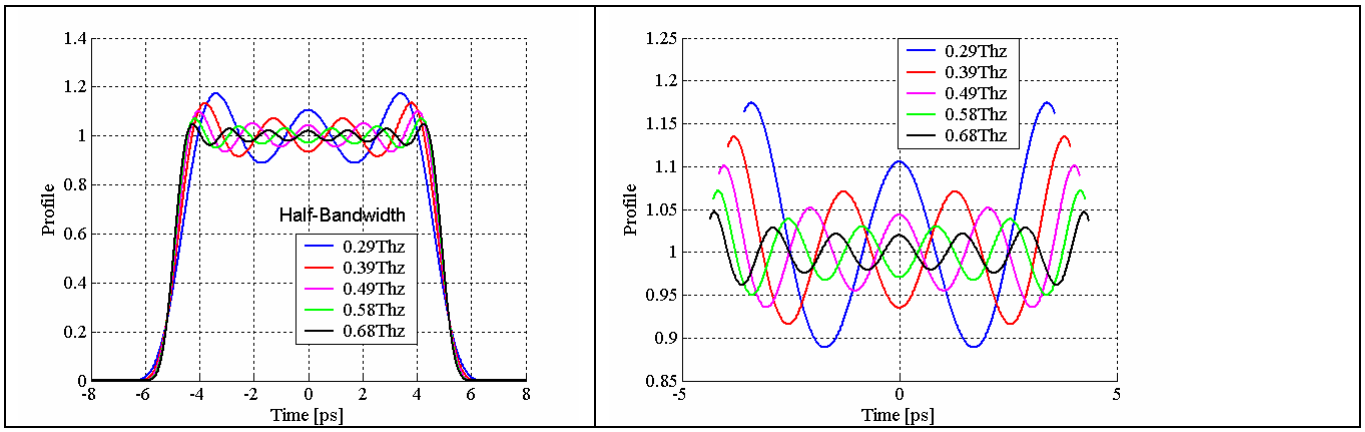

(a) (b)

Figure 2- a- Intensity Temporal Profile for a transform limited pulse (with cutoff or half bandwidth varying between 0.29THz and 0.68 THz) – b- plateau in (a) with expanded ordinate exhibiting relative amplitude of modulation.

The dependence of the rms amplitude for modulation on the plateau on the sideband cutoff frequency (half bandwidth) is also displayed more clearly in figure 3a. The reduction of the modulation amplitude with increasing cutoff for a given input rise/fall time is clear. Also shown is the modulation amplitude increase with reduced input rise/fall time for a given cutoff value. For example, for case of the 0.7 psec input and above 0.9 THz cutoff, the rms modulation amplitude is less than 1 %. In this case the cutoff needs to be at least 0.9 THz to keep the rms amplitude modulation less than or equal to 1%.

The LCLS injector drive laser system is expected to provide a range of uv pulse lengths between 5 and 20 ps. The transform limited modulation amplitude will vary for the different pulse lengths for a given cutoff value. For example, to maintain less than 1% rms amplitude modulation the cutoff frequencies are near 0.75 THz for a 20 psec FWHM and 0.95 THz for a 5 psec FWHM as displayed in figure 4.

(b) FWHM and Rise/Fall time

Spectral cropping also increases synthesized rise/fall times (to be distinguished from the input parameter values which are lower) and reduces the resultant FWHM below the input value of 10 ps. Figures 3b and 3c illustrate this dependence on the frequency cutoff (half bandwidth) value.

Also shown is the obvious result that the input rise/fall times and pulse duration (FWHM) are better preserved for higher cutoff frequencies. For example, for cutoff values above 1.5 THz, synthesized rise/fall times and FWHM are indistinguishable from the input values and the rms amplitude modulation is insensitive to the input rise/fall time.

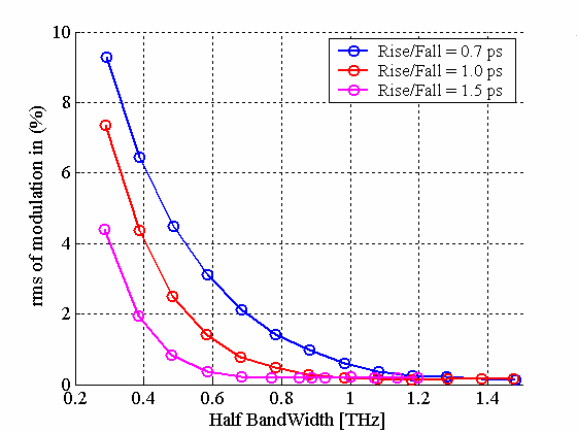

3(a)

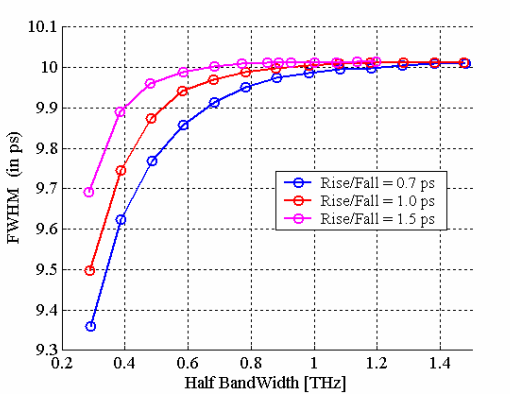

(3b)

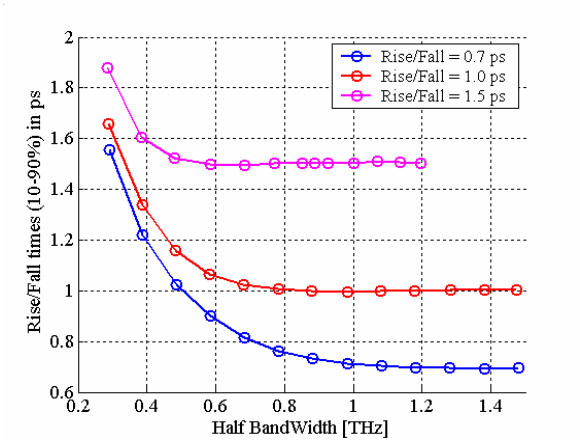

(3c)

Figure 3- (a) Dependence of the rms modulation on the half bandwidth.
(b) Synthesized pulse FWHM as a function of the half band width
(c) Rise/Fall time dependence on the half bandwidth for input rise/fall times of 0.7ps, 1ps, and 1.5ps

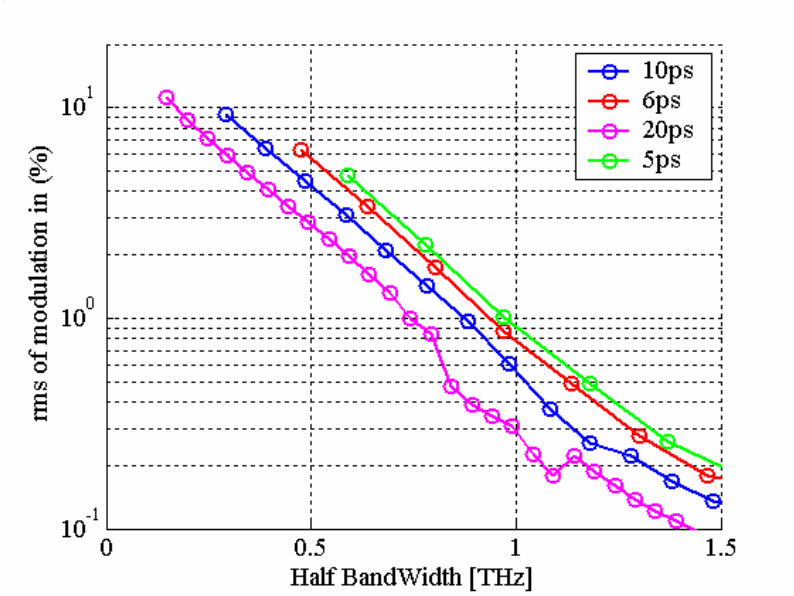

Figure 4 – Dependence of the rms of modulation amplitude on the half bandwidth for 4 different bunch lengths.

IV- Results from ASTRA simulations:

ASTRA simulations were done for the LCLS injector for three types of distributions maintaining the 10- psec FWHM. The three distributions were based on a 1.0 THz frequency cutoff with input rise/fall times of 0.7 ps, 1ps and 1.5ps. Only the 0.7ps and 1.5ps cases are shown.
Figures 5 and 6 show the development of the longitudinal space charge force instability along the injector beamline. It is initiated by the modulation on top of the plateau due to finite bandwidth. We show the longitudinal phase space at six locations: (1) at the gun exit , (2) at the entrance to L01 the first linac section, (3) 30 cm into L01, (4) 2m into L01, (5) at the entrance of L02, the second linac section, (6) at the end of L02. In the left hand side column, we show the longitudinal phase space. In the right hand side column, we show the longitudinal phase space after removal of the correlation up to order 5. One can see the development of the micro-bunching in that right hand side column, as it is very small compared to the total correlated energy spread.
Simulations agree with the theory when one evaluates the amplitude of oscillation of the centroid of the slices along the bunch in the longitudinal phase space. We are still uncertain as of the value of the uncorrelated energy spread. We believe it is likely that numerical noise artificially increases that quantity.
In the scope of our study, the comparison of figure 5 and figure 6 demonstrates that the oscillation amplitude of the slices centroid is larger for the fast rise/fall time than for longer one. It is 1.1 keV with a fast rise/fall time of 0.7 ps against 0.6 keV with a rise/fall time of 1.5 ps.
A 0.7 ps rise/fall time is desired for the LCLS. It has been demonstrated that even a very small oscillation would be dramatically amplified [2] in the chain of compressors

downstream the LCLS injector. Therefore, a “laser heater” has been included in the LCLS Injector beamline.

End Gun

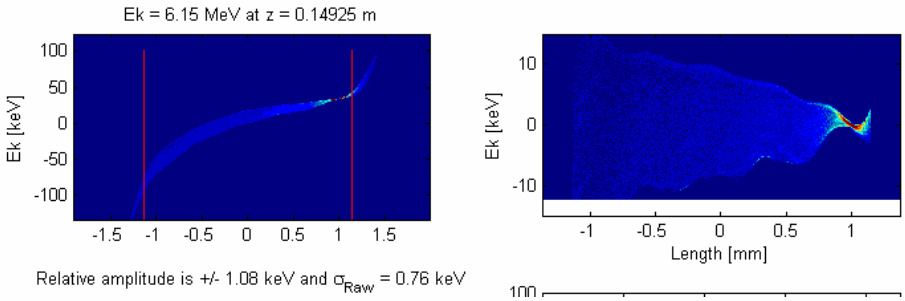

Entrance L01

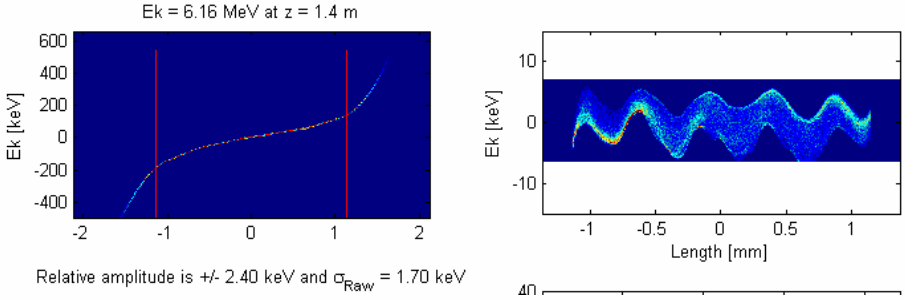

30cm in L01

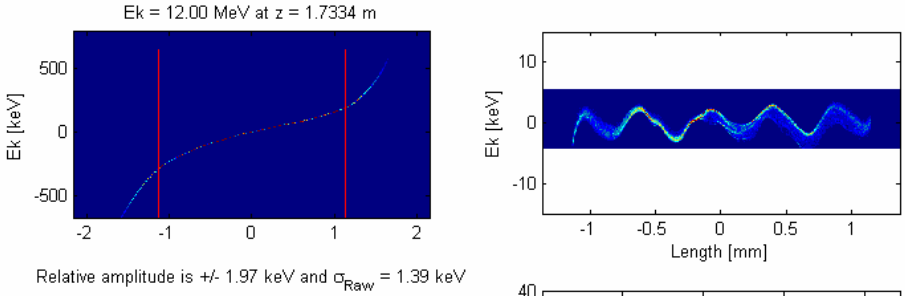

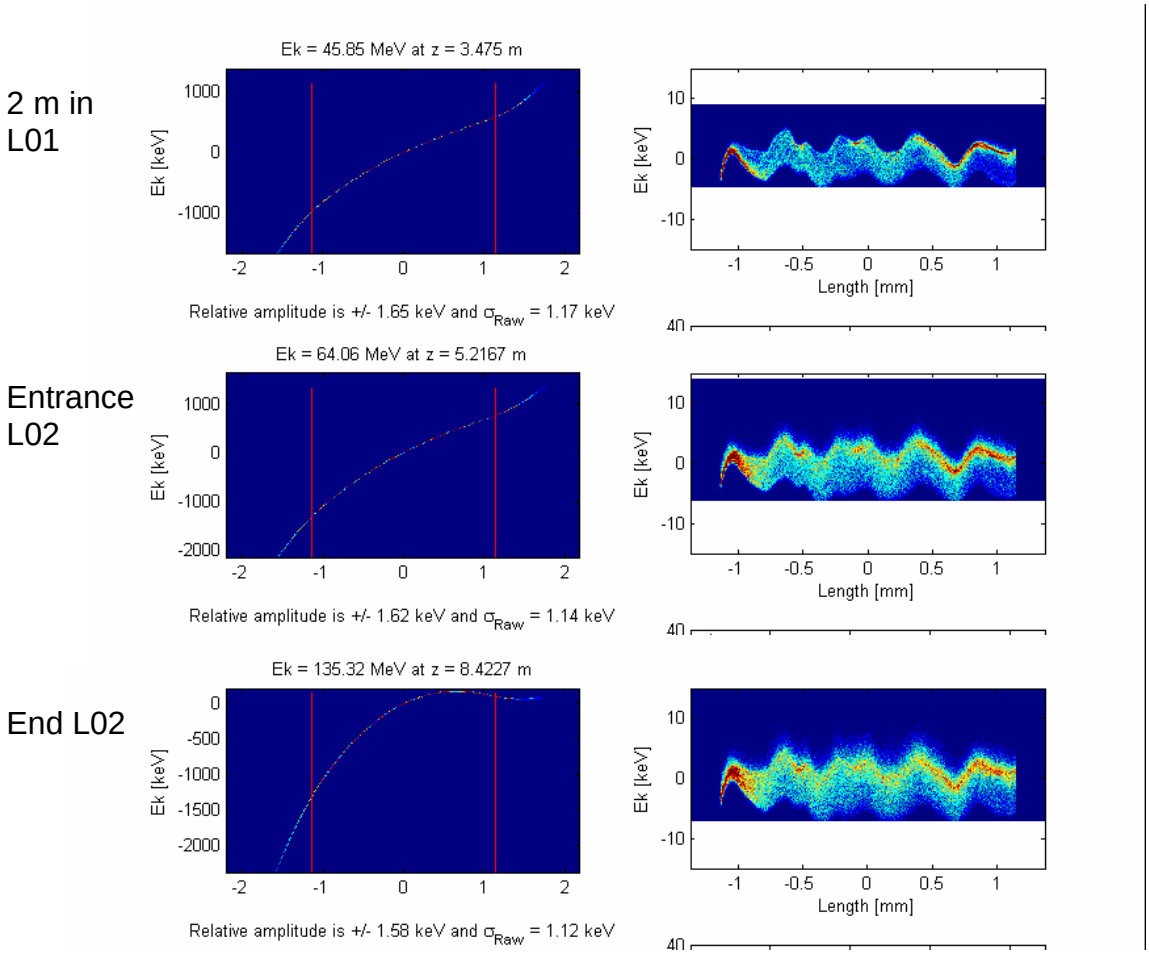

Figure 5- Evolution of longitudinal phase space along the electron beamline for a uv laser profile with rise/fall time of 0.7 ps and a 1.0 THz frequency cutoff;
Left plots show the longitudinal phase space with Energy Spread in keV vs longitudinal position within the pulse (in mm) for varying locations, z along the beamline
Right plots show the longitudinal phase space for the same parameters after removal of the correlation up to order 5

End Gun

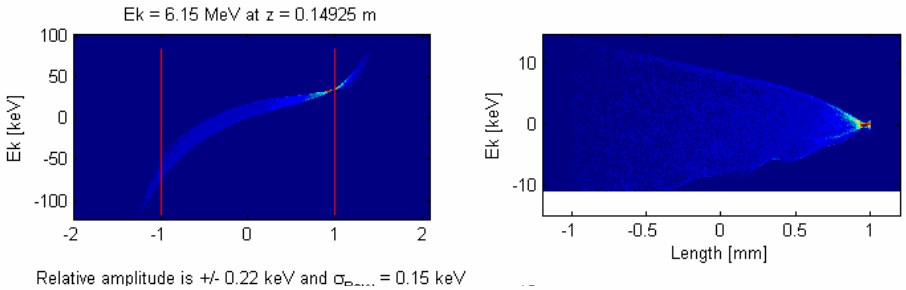

Relative amplitude is +/- 0.22 keV and σ_{Raw} = 0.15 keV

Entrance L01

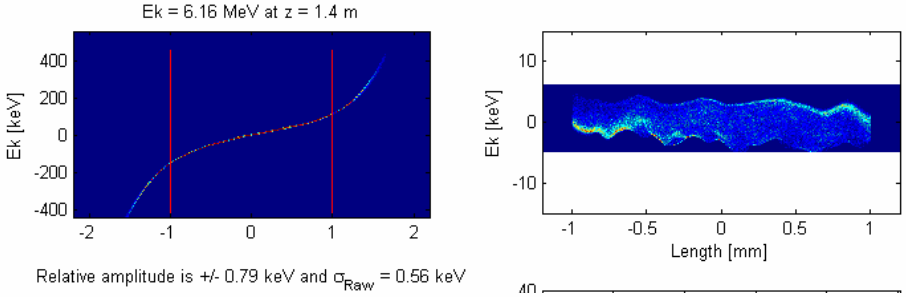

Relative amplitude is +/- 0.79 keV and σ_{Raw} = 0.56 keV

30cm in L01

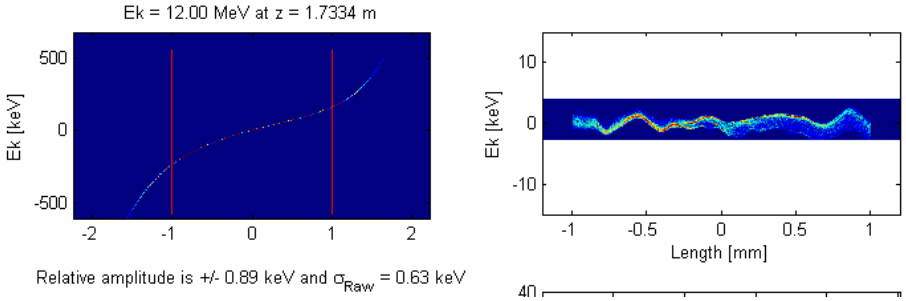

Relative amplitude is +/- 0.89 keV and σ_{Raw} = 0.63 keV

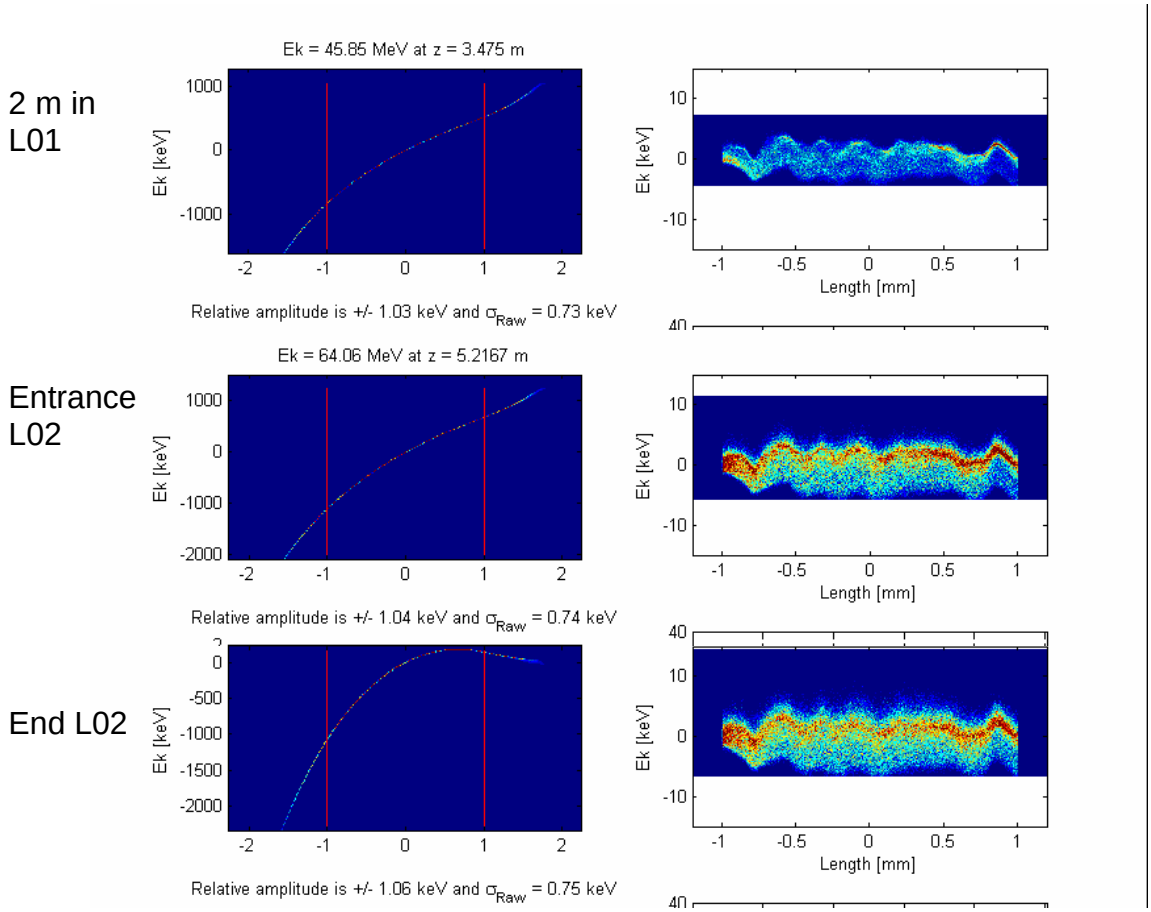

Figure 6 – The same as in figure 5 except the rise/fall time is increased to 1.5 ps

V- Discussion:

(a) IR Bandwidth Assessment:

Our analyses indicate that the uv frequency cutoff value (half bandwidth) should be at least 1.5 THz (i.e. include 14 positive sidebands).
With negative sidebands also considered, this is a full bandwidth of 3 THz about the central frequency value. While 3 THz corresponds to a full uv wavelength interval of 0.65 nm at 255 nm, it also corresponds to a full ir wavelength interval of 5.9 nm at the fundamental 765 nm wavelength (where we have used equation (1) and preserved the required number of sidebands in the uv and ir cases). The appropriate methodology here is to determine first the transform limited uv pulse bandwidth (i.e. FWHM) from considerations of injector beam parameters and behavior. The ir bandwidth can then be determined from the uv case with due consideration of uv transport and details of third harmonic generation (THG) using incident ir pulses with similarly shaped temporal profiles.

At ir intensity levels well below saturation, uv generation via THG is a third order process. The third order effect on the uv temporal shape at leading and trailing edges will be notable. Phase matching considerations, as determined by the crystal type and

thickness, limit the angular acceptance , spectral bandwidth, and temperature range for efficient THG (in addition to other factors) and can change the pulse shape. That is, the THG efficiency and pulse shaping affect each other. This is particularly true when the spectral bandwidth is significantly less than the incident ir bandwidth. These THG related details will be addressed in a Part II report and are not covered here.

(b) Spectral masking and bandwidth

Because we are addressing minimum bandwidth requirements, this report describes what we can expect from Fourier transform limited syntheses of laser pulse shapes (temporal profiles) by spectral masking alone. This would employ techniques similar to those described in [8 and 9] at ir wavelengths. We address the spectral requirements of the ir laser input to a spectral mask. To introduce this subject matter in a simplistic manner, we assume here, with regard to figure 1, that the ir and uv pulse envelope spectra differ only by the scaling of the central carrier frequency (which is a factor of 3 and equivalent to a THG spectral bandwidth that greatly exceeds the incident ir bandwidth).
The required FWHM spectral bandwidth of the ir laser pulse can be determined from a specified cut-off value, ν_c, if the functional form for the input single pulse spectrum is known. We assume a Gaussian spectrum, S for an arbitrary frequency, ν of the form:

$$S = \alpha\, S_o \exp\left(-4.(\ln 2).\left(\frac{\nu}{FWHM} \right)^2 \right) \qquad (3)$$

for which the minimum required FWHM is determined by ν_c and f according to :

$$FWHM \geq \nu_c \sqrt{\frac{4\ln 2}{\ln\left(\frac{\alpha}{f}\right)}} \qquad (4)$$

where f is the relative peak amplitude (relative to the peak value at the central ir frequency) of the sideband nearest the cutoff frequency and α is a frequency independent loss factor. This comparison of spectral masking requirements with the input pulse spectrum is displayed in the figure 7. For example, in the lossless case (α =1) with f in the range 0.0001 to 0.01, we require that the input spectral FWHM be at least 55% to 78% (respectively) of the cutoff value ν_c. This is slightly increased to the range 57% to 84% if the loss α is 0.5. Therefore, for ν_c = 1.5 THz, α =0.5 and f = 0.01, the ir FWHM spectral bandwidth must exceed 1.3 THz which corresponds to 2.5 nm at 765 nm. Figure 7 illustrates the Gaussian ir bandwidth requirements for the case, α = 0.5 and ν_c = 1.5 THz with f= 0.001. It is well known that dynamic range requirements shown in figure 7 can be met with spectral masking techniques.

(c) Spectral masking and resolution:

The precision with which transform limited ir envelopes can be synthesized by spectral masks alone must be addressed briefly Although details of the spectral masking technique is not the subject matter of this report, a few comments can be made. Weiner et al [9] have shown that an appropriate mask would be located in the midplane (Fourier plane of a focusing lens) of a conventional pulse stretcher apparatus set for zero dispersion. The stretcher design could include a diffractive grating pair, and a lens pair. In this plane it is the spatial dispersion of the spectral components, $\frac{\delta\lambda}{\delta x}$ that determines masking resolution and is given by:

$$\frac{\delta\lambda}{\delta x} \approx \frac{d\cos(\theta)}{F} \qquad (5)$$

where $\frac{1}{d}$ is the grating groove density, F is the lens focal length, and θ is the diffraction angle from the grating.
We suggest initially that each sideband should be spatially resolved into 10 elements. In this case, we would require 10 μm element resolution for the case $\frac{\delta\lambda}{\delta x}$ = 2 nm/mm (using F = 200 mm, θ = 45 ° and 1/d = 1740 grooves per millimeter). This can be accomplished with current photolithographic methods.

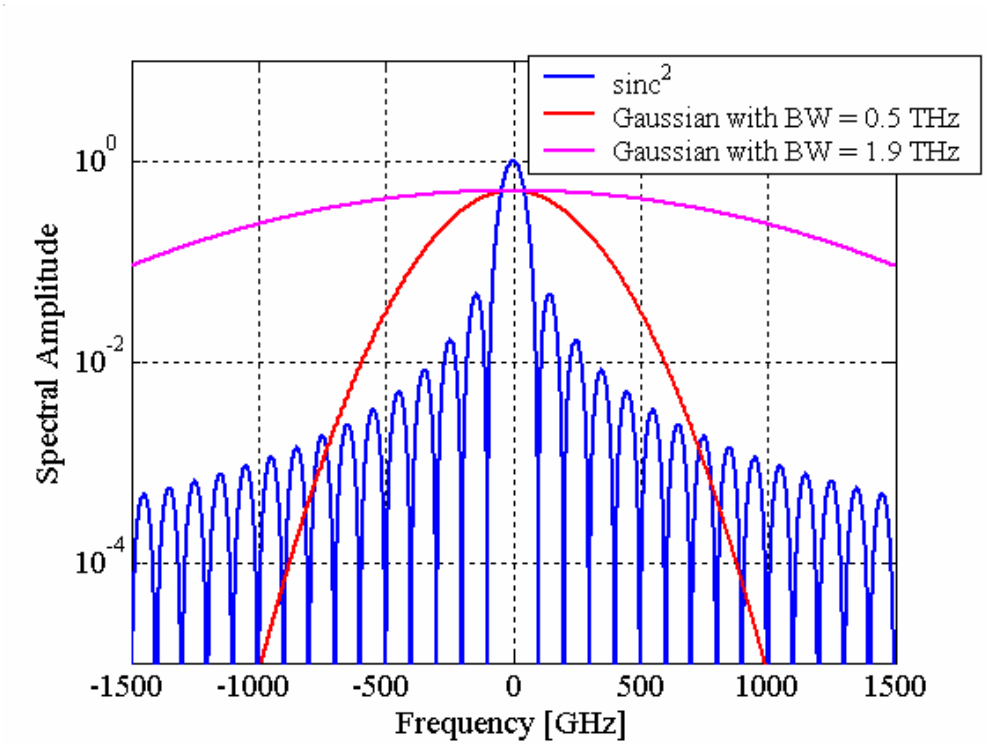

Figure 7 : Sideband limits of a $sinc^2$ spectrum imposed by a Gaussian input spectrum with a logarithmic ordinate. For the lower Gaussian curve, the FWHM bandwidth is 0.5 THz and for the upper Gaussian curve, it is 1.0 THz. The $sinc^2$ spectra is for the 10 ps FWHM flattop temporal profile.

(d) Comparison with Time slew variations at the Photocathode

The constraint on the rise/fall time is less critical than that on the amplitude noise in the plateau region. The rise/fall time requirements being 'softer' than anticipated means that we can accommodate slight variations in the time slew setting for the incident uv pulse which are still expected to be much less than nominal rise/fall time values.

For example, a reflective uv diffraction grating can be used to establish the following two critical uv pulse conditioning requirements: (i) the transverse spatial anamorphic compression needed to obtain a circular spot on the photocathode surface and (ii) the time slew or tilted amplitude front of the uv pulse needed for time delay compensation to guarantee that the uv waveform reaches the photocathode surface simultaneously across the full spot diameter at the photocathode. For the nominal incident angle of 72 degrees (with respect to the normal of the photocathode surface) and a single uv wavelength of 255 nm (zero bandwidth in this example), a one degree variation of the incident angle on the uv launch grating corresponds to about a 130 femtosecond variation in the time slew (about 2% of the ideal time slew value and 13% of a 1 psec rise/fall time). This time slew error is reduced slightly if the refracted angle off the grating (which is also the incident angle approaching the photocathode) is reduced slightly (for example, from 72 to 71 degrees). Because we assume that the uv pulse is

imaged from the grating to the photocathode these one degree angular variations have an insignificant effect on the transform limited uv bandwidth requirements with respect to rise/fall time.

VI- Conclusion:

This Part I report describes minimal uv spectral bandwidth requirements for synthesis of Fourier transform limited temporal profiles (with acceptable rise/fall time and modulation amplitude on a flat plateau) to guarantee generation of electron beams of acceptably low projected emittance for successful LCLS operation. Although candidate techniques for laser pulse shaping are not evaluated here it is noted that the programmable acousto-optic dispersive technique [6,7] reshapes pulse spectra (as does spectral masking) but fundamentally generates a chirped waveform for which the FWHM spectral bandwidth by definition exceeds the transform limit associated with the temporal profile of the pulse The pulse shaping techniques of choice will be determined largely by (i) the extent to which photocathode irradiation by a chirped waveform can generate electron microbunches with a flatopped current, (ii) the ease with which temporal flattop pulse shapes with adaptive control can be generated, (iii) the impact of pulse bandwidth on ir pulse amplification as well as on THG efficiency and uv pulse shaping and (iv) bandwidth limitations imposed by the requirements of uv transport to the photocathode. Ultimately, we can anticipate that an optimal combination of pulse shaping techniques might be used to establish desired pulse shaping with adaptive features. This hybrid approach would also incorporate the shaping effects imposed by ir amplification and may afford separation of the adaptive function from passive shaping processes to some degree. In Part II, we will address the transform limited case of nonzero slope in the plateau region for which this report would serve as a useful reference. Details of the THG process will also be examined to more accurately assess minimal bandwidth and temporal shaping requirements for incident ir pulses.

References:

[1] Z.Huang “Suppression of microbunching instability in the linac coherent light source” Topics
Phys. Rev. ST Accel. Beams 7, 074401 (2004)-
[2] Juhao Wu, P. Emma, Z. Huang, C. Limborg (SLAC), M. Borland (Argonne),. "Temporal Profile Of The LCLS Photocathode Ultraviolet Drive Laser Tolerated By The Microbunching Instability".LCLS-TN-04-6, Apr 2004. 6pp. Presented at 22nd International Linear Accelerator Conference (LINAC 2004), Lubeck, Germany, (16-20 Aug 2004)
[3] C.Limborg-Deprey et al. ”Computation of the Longitudinal Space Charge Effect in Photoinjectors” EPAC 04
[4] C.Limborg-Deprey et al “Longitudinal Space Charge Instability”, http://www.aps.anl.gov/asd/theory/talks/presentations-online.html

[5] J.A. Hoffnagle and C.M. Jefferson “Design and performance of a refractive optical system that converts a Gaussian to flattop beam”, Applied Optics / Vol 39. [30], 5488 (20 October 2000).
[6] C.Vicaro et al. “Preliminary results using an acousto-optic dispersive filter for laser pulse shaping” private communication
[7] F. Verluise et al., “Amplitude and phase control of ultrashort pulses by use of an acousto-optic programmable dispersive filter: pulse compression and shaping”, Opt. Lett. 25[8], 575 (April 2000).
[8] A.M. Weiner, “Femtosecond pulse shaping using spatial light modulators”, Rev. Sci. Inst. 71[5], 1929 (May 2000).
[9] A.M. Weiner et al., “High-resolution femtosecond pulse shaping” J.O.S.A. B5 [8], 1563 (August 1988).